International Journal of Vehicle Safety

ISSN online: 1479-3113 - ISSN print: 1479-3105
https://www.inderscience.com/ijvs

Pedestrian airbag folding patterns on airbag deployment and head injuries based on corpuscular particle method

Reza Deabae, Javad Marzbanrad

DOI: 10.1504/IJVS.2022.10054752

Article History:

Received:	17 October 2021
Accepted:	10 February 2022
Published online:	17 March 2023

Pedestrian airbag folding patterns on airbag deployment and head injuries based on corpuscular particle method

Reza Deabae and Javad Marzbanrad*

Vehicle Dynamical Systems Research Laboratory,
School of Automotive Engineering,
Iran University of Science and Technology,
Tehran, Iran
Email: reza.deabae@gmail.com
Email: marzban@iust.ac.ir
*Corresponding author

Abstract: An earlier study by authors implemented Corpuscular Particle Method (CPM) for simulations of Pedestrian Protection Airbags (PPA). Present study utilised the CPM to investigate the effect of gas flow on the airbag's unfolding procedure. A PPA was designed to cover bottom of windshield and A-pillars where pedestrian head is more likely to hit and stiffness is high. This paper aims to investigate the effect of six folding patterns on PPA deployment behaviour and pedestrian head injuries. For each folding pattern, headform impact on nine points was simulated. Head acceleration curves, HIC values, PPA pressure and friction curves were exported. Results show that a PPA can reduce pedestrian head injuries by up to 90%. Across six patterns studied in this research, the folding-rolling as the best pattern generates lowest HIC values and the rolling-folding and rolling-stochastic as the weakest patterns generate high HIC values as they have higher friction.

Keywords: pedestrian safety; pedestrian airbag; corpuscular particle method; airbag folding; folding patterns; vehicle-to-pedestrian crash; passive safety; head injury.

Reference to this paper should be made as follows: Deabae, R. and Marzbanrad, J. (2022) 'Pedestrian airbag folding patterns on airbag deployment and head injuries based on corpuscular particle method', *Int. J. Vehicle Safety*, Vol. 12, Nos. 3/4, pp.226–252.

1 Introduction

According to World Health Organization (WHO) (2018) report on road traffic fatalities, pedestrians represent about 23% of street traffic fatalities extensively. A possible explanation for such a high proportion of road fatalities could be the emphasis put on occupant safety in past decades. Hence, vehicle configuration streamlined, for the most part, dependent on the security of people inside the vehicle. Although many efforts have been taken to reduce pedestrian fatalities in collisions, pedestrian crashes yield high fatality rates by up to 3% in comparison to vehicle occupant fatality rate, which is about 0.44% (Choi et al., 2016).

A substantial portion of pedestrian accident researches is focused on different scenarios of collision and contrasting pedestrian states. For instance, it is found that the pedestrian injury level is different for various gait stances (Zou et al., 2020). Liu et al. (2019) employed an orthogonal experimental design and analysis of variance to find significant factors that affect the dynamic response and injuries of pedestrian heads in the scenarios with head hitting the windshield. They reported that pedestrian orientation, collision velocity and vehicle type was found to be the most influential parameters on the dynamic response of pedestrian head and HIC value (Liu et al., 2019). In another research conducted by Sun et al. (2019), a total of 14,236 crash cases were investigated using Latent Class Cluster (LCC) and Multinomial Logit (MNL) methods. They have tried to specify the statistical relationship between pedestrian injury severity and contributing factors like built environment, crash characteristics and pedestrian behaviour. Sun et al. (2019) found out that pedestrian alcohol or drug involvement and senility could cause fatal and severe crashes. Additionally, it is reported that a significant portion of vehicle-pedestrian collisions occur away from urban intersections (Sun et al., 2019). Also, some other researchers investigated pedestrian-vehicle interactions, which lead to a collision (Chen et al., 2019; Han et al., 2017).

Anthropometric parameters investigation and creating new Finite Element (FE) models of dummies also attracted some attention in this field of study. For example, Lalwala et al. (2019) employed a THUMS human FE model to reconstruct and simulate some real-world pedestrian accidents to assess the stability and bio-fidelity of the THUMS human model (Lalwala et al., 2019). Pak et al. (2019) identified a vacuity of a high-stature pedestrian collision, so they developed a male 95th percentile pedestrian FE model. Researchers validated the model in vehicle-pedestrian impact simulation (Pak et al., 2019). Anthropometry of the pedestrian, front end shape of the vehicle and pre-impact states' influence on pedestrian kinematics and injury studied by Untaroiu et al. (2018a). Most of the analysis on the vehicle to pedestrian crash has been conducted with a focus on adult pedestrian anthropometry. Yet, to make non-adult pedestrian crash analysis possible, Meng et al. (2017, 2016) developed a 6-years-old child pedestrian finite element model by morphing a 5th percentile female pedestrian model. Moreover, several other studies have been conducted to investigate anthropometric parameters of pedestrians or to develop and evaluate FE dummy models (Decker et al., 2019; Untaroiu et al., 2018b; Pak et al., 2018).

To reduce pedestrian mortality in traffic accidents research efforts on pedestrian injury mechanisms have been conducted for decades. Many kinds of research have been carried out on the redesign and modification of passenger car front shape and material to reduce the injury level. Vyas et al. (2019) proposed the concept of using active stiffness control composites in the bonnet to satisfy both bonnet's structural requirements and reduce pedestrian head impact injuries. They made a bonnet which consisted of an aluminium outer shell and an inner hood structure made out of Active Stiffness Control (ASC) Carbon Fibre Reinforced Polymer (CFRP). The bonnet enables stiffness reduction of the hood structure for head impact mitigation in the event of a collision with a vulnerable road user (Vyas et al., 2019). An optimisation method for vehicle front shape has been proposed by Li et al. (2017) to minimise pedestrian injuries in a vehicle-pedestrian crash. They reported that a safe vehicle for overall pedestrian safety ought to have a broad and slick bumper, the height of bonnet leading edge equal to 750 (mm), a bonnet with short length of less than 800 mm, as well a shallow bonnet (either >17° or <12°) and a planar windshield (≤30°) (Li et al., 2017). Yüksel et al. (2017) used an

aluminium bonnet instead of a steel bonnet and evaluated its effect on HIC value while a headform impacts the hood. They also proposed an evaluation method for pedestrian head impact on the bonnet using simulation and experimental tests (Yüksel et al., 2017). The effect of lower bumper shape on pedestrian leg injuries also has been studied by Wetzstein et al. (2015) using a Flex-PLI leg impactor. They optimised bumper shape to decrease the level of lesion obtained by calculating knee ligament extensions and tibia bone bending moments (Wetzstein et al., 2015). Zeng et al. (2014) also proposed a design optimisation method for bonnet inner to reduce the severity of trauma. In their research, an optimisation method that targets both bonnet's structural stiffness and pedestrian head protection is implemented (Zeng et al., 2014).

According to Longhitano et al. (2005) it is found that for cars, the head is the region of the body most often injured. Also, injuries to the head in a vehicle-pedestrian collision are predominately associated with windshield, A-pillars, and the upper part of the bonnet (Beles et al., 2019; Longhitano et al., 2005). So, it is evident that protecting pedestrians' heads in a vehicle-pedestrian accident is of high importance. A high portion of vehicle-pedestrian crash analysis has been conducted to modify and optimise the materials, front-end geometry and structure of the car. On the contrary, there is a limitation on modifying and optimising the front-end properties because it may cause vehicle occupant safety debilitation (Lim et al., 2014; Zeng et al., 2014). Consequently, two kinds of pedestrian protection systems were introduced, passive and active safety systems.

1.1 Pedestrian protection systems

There are two types of pedestrian safety systems, active safety systems and passive safety systems. Active safety systems such as Autonomous Emergency Braking (AEB) attempt to prevent a crash by providing advanced warning information or controlling vehicle manoeuvre automatically. In active methods, the system tries to detect obstacles using different vision systems or radar systems. Once an obstacle, either pedestrian or non-pedestrian, is detected, other operational systems like AEB, Dynamic Brake Support (DBS), Autonomous Emergency Steering (AES) and Emergency Steering Support (ESS) try to activate the brake system autonomously or steer the vehicle to alter the vehicle path and potentially avoid the collision. In some cases, because of the diversity of the surrounding environment of a vehicle and the instability of the feedback system in the vehicle, the effectiveness of the vehicle-to-pedestrian distance detection system is insufficient, which leads to collision injury (Lu et al., 2020). Although, once a collision is inevitable, passive safety technologies aim to minimise pedestrian injury. Thereupon, two pedestrian protection systems have been proposed which do not require vehicle front-end modification; therefore, they would not result in occupant safety deterioration. These systems consist of a pedestrian protection airbag and a pop-up hood.

1.1.1 Pop-up hood

In passive methods, collision detection systems are employed to detect a collision, and in case of a pedestrian-vehicle crash, it activates passive safety systems. A pop-up hood is then activated to raise the rear section of the hood that makes a distance between the bonnet and other stiff parts in the engine compartment. Hence, the system creates a secure space for the bonnet to damp the energy of the impact. As stated by Krenn et al.

(2003) it is suggested to use a kinematic hood to reduce pedestrian injuries. It is observed that the hood deployment provides space for deformation during an impact; therefore, the hood can absorb more energy (Krenn et al., 2013). Nagatomi et al. (2005) proved the effectiveness of the pop-up hood system by conducting a simulation of a vehicle impacting a full-scale POLAR dummy. Their research showed that using a pop-up hood system for pedestrian protection can reduce HIC values by approximately 30% (Nagatomi et al., 2005). Furthermore, some other researches have been carried out on the analysis and design of the pop-up hood. Shin et al. (2008) used an orthogonal array to optimise pop-up hood performance by minimising the summation of HIC value in five different points located on the bonnet; the optimisation objectives of their research were hinge thickness, actuator material, actuator thickness and actuator angle. This parameter optimisation could reduce HIC values by 16.7% inclusively (Shin et al., 2008). Huang and Yang (2010) conducted a pop-up hood optimisation using Response Surface Method (RSM) to find out optimum values for material stiffness, lifting velocity and lift height of the pop-up hood. Their optimised model was found to be able to decrease pedestrian head impact responses and to reduce HIC value to less than 1000 (Huang and Yang, 2010).

Takahashi et al. (2013) developed a pressure chamber to sense and differentiate the collision to pedestrians or other obstacles. Additionally, Takahashi et al. (2013) designed a push rod type actuator that is capable of absorbing the impact energy by bending at the impact time. Figure 1 shows a pop-up hood system in action while the rear of the bonnet is lifted and the pedestrian head is striking the lifted hood. This mechanism can prevent the pedestrian headfrom impacting other dense parts and regions under the hood. Lee et al. (2018) investigated the effect of the pop-up hood system experimentally and reported that this passive safety feature could reduce HIC by up to 40%.

Figure 1 Headform impacting a vehicle bonnet equipped with a pop-up hood

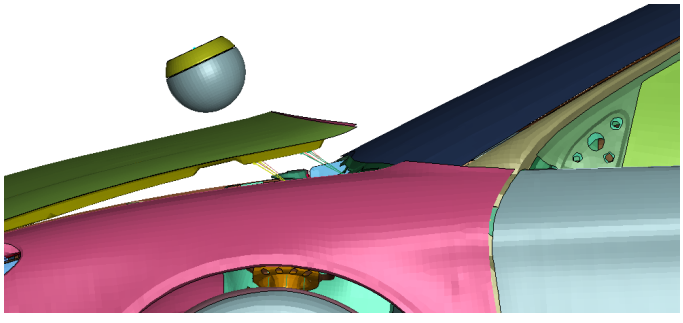

1.1.2 Pedestrian protection airbag

The Pedestrian Protection Airbag (PPA) system was first developed and introduced by Volvo in 2012. The first vehicle equipped with this technology was Volvo V40 (Jakobsson et al., 2013). Severy (1970) shared the idea of protecting a pedestrian in a vehicle-pedestrian crash by an inflatable cushion in the early 1970s. This system consists of housing, an inflator, and an airbag cushion. At the moment that a vehicle to pedestrian crash has been detected either by pressure sensors in the bumper or other detection devices, the system first activates the hood hinge release mechanism and deploys the

pop-up hood system, then pedestrian protection airbag is deployed. The pedestrian protection airbag module generally installs near the bonnet rear so that it can protect the pedestrian headfrom contacting the bottom of the windshield and A-Pillars when deployed. Deployed pedestrian airbag covers the lower end of the windshield and A-pillars to preserve the pedestrian headfrom contacting such stiff parts. Figure 2 shows how a pedestrian airbag was installed on the bonnet. Lim et al. studied pedestrian protection airbag and pop-up hood systems. Their research indicated that using pedestrian safety systems such as pedestrian protection airbag and pop-up hood can improve the vehicle's pedestrian protection significantly without altering the vehicle's front end structure. Moreover, the HIC values on the bottom of the windshield and the A-pillars could be reduced by up to 95% (Lim et al., 2014). Yang et al. (2015) studied the effect of inflator type, folding method and height of the PPA on pedestrian injury using the Wang-Nefske method. Their research showed that rolling and then folding the PPA can improve the stability of the airbag and deployment velocity due to less resistance to gas inflation. Also, the centre spurt type inflator due to smooth gas flow is more reliable than the bottom spurt type. Additionally, a PPA with a small height showed better performance when the headform hit the end of the PPA; however, the HIC value was lower in the centre of PPA while using large height PPA (Yang et al., 2015). Recently, Lu et al. (2020) also proposed an all-around front-end airbag that is capable of covering the hood and the bottom of the windshield simultaneously. They reported that using an all-around front-end airbag could decrease the maximum value of HIC by 66.7% and effectively reduce the collision damage (Lu et al., 2020).

Figure 2 Pedestrian protection airbag unit installed on the bonnet inner

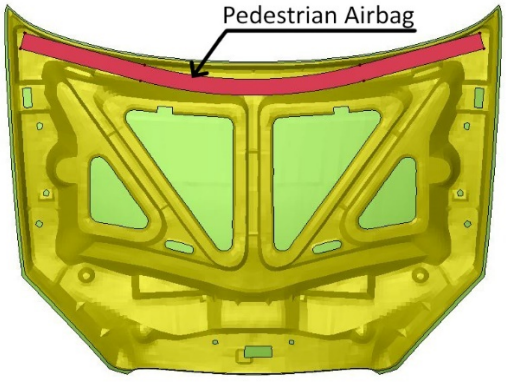

1.2 Airbag simulation methods

Simulating airbag deployment could be done using three different methods, the CV method, the ALE method, and the corpuscular particle method. The known Wang-Nefske method developed by Wang and Nefske (1988) in the late 1980s is a UP formulation for airbag simulation purposes. Rather than the UP method, an Arbitrary Lagrangian-Eulerian (ALE) approach is also developed that models both the gas entering the bag and one surrounding it. Also, in the Corpuscular Particle Method (CPM) the gas flow is modelled as individual particles.

1.2.1 Uniform pressure method (UPM)

The Wang-Nefske approach, also known as the Uniform Pressure (UP) method, is a highly simplified process model that mostly ignores the local fluid effect (Hirth et al., 2007). While in a regular driver or passenger airbag, the airbag deployment process is of lower importance due to the impact occurrence with a completely deployed airbag; but it is entirely different for Out Of Position (OOP), which airbags dynamic behaviour may come into account. A similar is true when speaking of PPA or curtain airbags, and a correct physical model of the gas flow and its effect on airbag unfolding is needed. In the UP method, the Gaussian integral theorem is used to calculate the volume of the airbag in each time step, then the pressure (p) is determined on the basis of the ideal gas law and an adiabatic process as a function of density (ρ). Defining the isentropic coefficient $\left(\gamma = {C_p}/{C_v}\right)$ and internal energy $\left(e = {E_{INT}}/{\rho_0}\right)$:

$$p = (\gamma - 1).\rho.e \tag{1}$$

Based on this definition for two adjacent deformation states:

$$\frac{e_2}{e_1} = \left(\frac{V_1}{V_2}\right)^{\gamma} = \left(\frac{\rho_2}{\rho_1}\right)^{\gamma} \tag{2}$$

According to Wang and Nefske (1988), three elements of the overall inflating mass flux are as follows:

$$\dot{m}_{tot} = \dot{m}_{in} + \dot{m}_{out} = \dot{m}_{12} + \dot{m}_{23,vent} + \dot{m}_{23,prosity} \tag{3}$$

The rise in internal energy due to incoming and outgoing gas to the bag is written as follows:

$$\dot{E} = C_p\left(\dot{m}_{in}T_1 + \dot{m}_{out}T_2\right) - p\dot{V} \tag{4}$$

1.2.2 Arbitrary Lagrangian-Eulerian method (ALE)

In the ALE approach, a discretised model of air surrounding the airbag and the gas flow, as well as coupling forces, are necessary to be considered. The observer may follow his own arbitrarily defined path in space in an ALE-based approach. Mathematically an arbitrary reference area in the conservation laws leads to an additional term as equations (5) to (7); where v denotes the velocity of the material, $\dot{x}$ is the velocity of the moving grid, $\ddot{x}$ is its acceleration, parameter b is the external body forces, D represents the constitutive tensor, ρ is the density of the gas, u represents the kinetic energy and q is the additional heat source (Hirth et al., 2007):

$$\rho\ddot{x} + \rho\nabla\dot{x}\left(\mathrm{v} - \dot{x}\right) = \rho b + div\sigma \tag{5}$$

$$\dot{\rho} + \nabla\rho\left(\mathrm{v} - \dot{x}\right) + \rho\, div\,\mathrm{v} = 0 \tag{6}$$

$$\rho\dot{u} + \rho\nabla u\left(\mathrm{v} - \dot{x}\right) = \sigma : D + \rho\mathrm{r} - \nabla\mathrm{q} \tag{7}$$

Besides the gas dynamic effects, the unfolding of the airbag in the ALE system leads to another algorithmic problem that needs to be considered. The missing link between the two separate discretisation schemes must be addressed by an acceptable coupling mechanism that solves the problem of contact between the gas and the airbag fabric.

ALE algorithm prevents synthetic leakage due to the fact that it does not contain porous flow through the fabric, and this conflicts with the wish to calculate porous effects in this approach. Consequently, an experimentally determined curve that describes the flow velocity through the fabric as a function of pressure difference is defined to calculate the mass loss by subtracting the curve value from the system, and a heat source balances the kinetic energy in conservation laws.

1.2.3 Corpuscular particle method (CPM)

The concept of the Corpuscular Particle Method (CPM) is based on the kinetic molecular theory. That is a set of assumptions regarding gas behaviour on the molecular level that leads to the ideal gas law on a macroscopic statistical level. The Fluid-Structure Interaction (FSI) treatment in this approach is simplified as the corpuscular particle method is a Lagrangian approach. Also, the lack of field equations significantly simplifies the development of the robust numerical implementation of the governing equations (Olovsson, 2007). The theory is based on the idea that Daniel Bernoulli (1738) proposed that stated discrete molecular collisions build up the air pressure against a piston. Then, James Clerk Maxwell (1860) derived an expression for the molecular velocity distribution at thermal equilibrium. The kinetic molecular theory is based on these assumptions:

- The average distance between the molecules is large compared to their size.
- There is a thermodynamical equilibrium, i.e. the molecules are in random motion.
- The molecules obey Newton's law of motion. Relativistic and quantum mechanical effects are negligible.
- The only molecule-molecule and molecule-structure interactions are perfectly elastic collisions.

The frequency of a single molecule's collisions to the wall of a rectangular box in positive *x*-direction could be calculated using this theory. Assuming the dimensions of the box to be equal to L_x, L_y and L_z along with molecule mass m_i and its velocity $v_i = \left[v_{x,i}, v_{y,i}, v_{z,i} \right]^T$ the frequency of impact $\left(f \right)$ can be calculated as equation (8). According to previously mentioned assumptions, the molecule-structure impacts are considered elastic, hence, transferred impulse at each impact $\left(j_{x,i} \right)$ is calculated as equation (9). The total impulse transferred over time equals to $J_{x,i}$ (see equation (10)). Assuming $A = L_y L_z$ as the area of the wall, $V = L_x L_y L_z$ as the volume of the box and $\left(N \right)$ number of particles, the pressure of the wall becomes $\left(p_x \right)$ (see equation (11)):

$$f = \frac{\left| v_{x,i} \right|}{2L_x} \tag{8}$$

$$j_{x,i} = 2m_i \left| v_{x,i} \right| \tag{9}$$

$$J_{x,i} = \int j_{x,i} t = \frac{m_i v_{x,i}^2 t}{L_x} \tag{10}$$

$$p_x = \frac{1}{V} \sum_{i=1}^{N} m_i v_{x,i}^2 \tag{11}$$

The kinetic energy will be evenly distributed between Cartesian directions at thermal equilibrium. So, considering $\overline{v^2}$ as mean-square of the molecular velocities and $\overline{v_x^2}$, $\overline{v_y^2}$ and $\overline{v_z^2}$ as mean-square velocities in each Cartesian direction will give equation (12). Combining equations (11) and (12) will calculate the pressure (p) where (m) is the total mass of the molecules, (W_k) is the total translational kinetic energy of the particles and (w_k) is the specific translational kinetic energy (see equation (13)).

$$\overline{v_x^2} = \overline{v_y^2} = \overline{v_z^2} = \frac{1}{3}\overline{v^2} \tag{12}$$

$$p = p_x = \frac{1}{V} \sum_{i=1}^{N} m_i v_{x,i}^2 = \frac{1}{3V} m\overline{v^2} = \frac{2W_k}{3V} = \frac{2}{3} w_k \tag{13}$$

So, a direct relationship between pressure and specific translational kinetic energy at thermodynamic equilibrium can be observed. From the macro-scopical point of view, translational kinetic energy is a fraction of the internal energy of the gas. For a mono-atomic gas, the specific translational energy (w_k) is equivalent to specific internal energy (e), i.e. no energy is stored as molecular spin or vibrations. Hence, equation (14) will be extracted.

$$p = \frac{2}{3}\frac{W_k}{V} = \frac{2}{3} w_k = \frac{2}{3} e \tag{14}$$

$$p = \left(\frac{C_p}{C_v} - 1 \right) e \tag{15}$$

In an ideal gas with constant heat capacities, pressure can be expressed as equation (15). Hence from equations (14) and (15), it can be concluded that for a mono-atomic gas $\gamma = C_p / C_v = 5/3$.

Taking the adiabatic expansion into account, it can be concluded that a particle inside a slowly expanding box loses some energy each time it impacts the moving wall. The value of energy drop (ΔE_i) can be calculated as equation (16). Combining this with the frequency of the impact (see equation (8)) will produce a rate of dropping energy $(\dot{E}_i)$ as equation (17). Where (v_p) is the velocity of the moving wall. Having (N) particles inside the box, the total rate of dropping energy due to impacts against the moving wall becomes $(\dot{E})$ as stated in equation (18):

$$\Delta E_i = \frac{1}{2} m_i \left(v_{x,i} - 2v_p \right)^2 - \frac{1}{2} m_i v_{x,i}^2 \approx \left| v_p \ll v_{x,i} \right| \approx -2 m_i v_{x,i} v_p \tag{16}$$

$$\dot{E}_i = f \Delta E_i = -\frac{m_i v_{x,i}^2 v_p}{L_x} = -m_i v_{x,i}^2 \frac{\dot{V}}{V} \tag{17}$$

$$\dot{E} = \sum_{i=1}^{N} \dot{E}_i = -\sum_{i=1}^{N} m_i v_{x,i}^2 \frac{\dot{V}}{V} \rightarrow \left| Equation(12) \right| \rightarrow = \frac{2W_k}{3} . \frac{\dot{V}}{V} \tag{18}$$

As mentioned previously, the total kinetic energy (W_k) is a fraction (ξ) of the total energy (E) which for a mono-atomic gas $\xi = 1$. Hence, equation (19) can be derived from equation (18). Where V_0 and V_t are volume of the box at time 0 and t, respectively. The exponent $\frac{2\xi}{3}$ is actually equivalent to $\gamma - 1$. Hence, the fraction of internal energy stored as translational kinetic energy can be expressed as equation (20):

$$\dot{E} = -\frac{2\xi E}{3} . \frac{\dot{V}}{V} \rightarrow \left| \begin{matrix} assume\, temprature \\ dependant\, \xi \end{matrix} \right| \rightarrow E(V_t) = E(V_0) \left(\frac{V_0}{V_t} \right)^{\frac{2\xi}{3}} \tag{19}$$

$$\gamma - 1 = \frac{2\xi}{3} \rightarrow \xi = \frac{3}{2} (\gamma - 1) \tag{20}$$

Temperature (T) is proportional to the translational kinetic energy of the molecules, as stated in equation (21), where M is the molar weight of the gas, and $R = 8.3145\,\text{J/molK}$ represents the universal gas constant.

$$T = \frac{M \overline{v^2}}{3R} \tag{21}$$

It can be seen that using equation (21), given temperature data at the inflator nozzle could be converted to molecule or particle total velocity and then equation (12) calculates velocity distribution in different Cartesian directions. These velocity elements next will be used to calculate energy, energy drop, pressure, impulse and frequency of particle's impact.

As it is not realistic to model every single molecule in the gas inside an airbag (roughly 10^{23}–10^{24} molecules), the concept suggests modelling the gas as individual particles so that each particle represents many molecules, as shown in Figure 3. Consequently, the pressure is calculated by the translational kinetic energy of the gas particles assuming that the translational kinetic energy of each particle equals the total kinetic energy of representing molecules.

Figure 3 Corpuscular particle method (CPM) concept

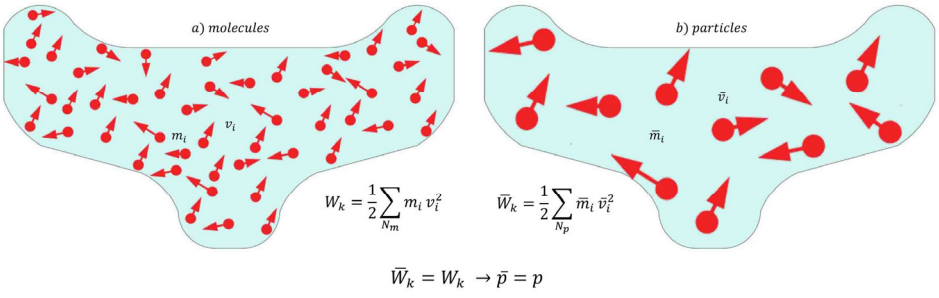

Hirth et al. (2017) compared three methods for airbag simulation to show the ability and benefits of each method. They showed that the CV method, also known as the Uniform Pressure (UP) method, could be used as a rough approximation of the airbag behaviour. Regarding their report, while simulating simple airbags without folding, vent holes and nozzle movements, all three methods lead to approximately similar results. Nevertheless, when vent hole, nozzle movement and specifically airbag folding come into account, results generated by each method differs from the others.

As another difference in the UP method, the vent hole is activated from the beginning of the inflation, while in CPM, the vent hole may be covered in the first stages; in other words, the blockage could be taken into account using CPM. As mentioned in the ALE method, no visualisation of venting gas is possible due to the internal removal of gas.

As another advantage of CPM Hirth et al. (2017) reported that CPM could manage the unfolding of the airbag better in comparison to other methods due to the fact that there are individual particles that could be sent through tight gaps, which will consequently open the airbag from both sides, while in the ALE approach before the tube has opened to a specific level because of the missing capability of gas flow to reach upfront regions, the folded tube opens up one element row by another. ALE shows the lower unfolding velocity in comparison to the experimental results, while in the CPM approach, an acceptable agreement is represented (Hirth et al., 2007). Additionally, Anantharaju et al. (2020) evaluated the maturity of CPM for capturing realistic deployment kinematics, accurate prediction of airbag pressure and reaction force for static airbag deployments. They also assessed the prediction accuracy of the impactor force for resting drop tower tests. Drop tower test was designed to represent an early interaction of potential occupant with an unfolding airbag as well as continued interaction with a fully deployed airbag. They reported that CPM could accurately predict the airbag pressure, reaction force and impactor force, suggesting that it is a suitable modelling method for airbag simulations (Anantharaju et al., 2020)

Also, regarding Hirth et al. (2017), there has been a significant difference in computing time between the three methods. The UP method seems to be less time consuming due to its simplifications. The ALE method though showed the highest computing time in different examples, where CPM was able to solve the problems up to 9 times faster than the ALE method.

In addition to Hirth et al. (2017) some other researchers also approved that the CPM has various advantages over the other two methods. Olovsson (2007) reported that the CPM has its advantage in situations of complex gas-structure interaction. Mroz and

Pipkorn (2007) stated that the particle-based algorithm is capable of handling complex folds, wrinkles and fine elements that are the requirements of pragmatic airbag modelling. Furthermore, reported by Lian et al. (2008) CPM does not have any difficulty interacting with tethers inside an airbag; this often causes problems in ALE models. Moreover, according to Wang and Teng (2010), the CP method was considered to be numerically straightforward and reliable because of the fact that the CP algorithm does not solve the field equations. As well, Yang et al. recognised that the CV model is less useful for simulating airbag early deployment applications such as OOP simulation. ALE is able to capture the dynamics of the airbag's initial deployment, but it is CPU intensive and complex to set up; on the other hand, CPM has similar simulation accuracy as the ALE model but needs much fewer CPU resources (Yang and Beadle, 2015). According to Lin et al. (2014) and Lin and Cheng (2018) a good correlation between test and numerical simulation results for airbag pressure and headform deceleration history was observed.

In summary, the corpuscular particle method has consistently been demonstrated to be very suitable for simulating airbags, particularly in the case of a combination of a wall to wall contact and high pressure. Besides, if the gas flow needs to be bent along sharp corners, the new approach can catch the primary effect with the same discretion, while a much finer Eulerian grid has to be selected for ALE (Hirth, et al., 2007). Furthermore, for similar or better results, a notable reduction in simulation time was observed in the CPM approach (Mroz and Pipkorn, 2007). Not to mention that there are also some limitations reported for this method. It needs a very detailed model of the airbag, which may result in a higher lead time to update the model for any major design or fold changes in airbag design and development applications. Also, the airbag pressure calculated by CPM was found to be typically higher than the test measurement in the early stages of airbag deployments (Anantharaju et al., 2020).

1.3 Head Injury criterion (HIC)

In a vehicle to pedestrian crash, lower extremities and the head are the most seriously injured regions; thus, several criterions are defined to evaluate injury level. The Head Injury Criterion (HIC) and Severity Index (SI) are the two critical measures for head injury evaluation. Equations (22) and (23) show the formulation of SI and HIC. Where the parameter $a(g)$ in equation (23) is the resultant acceleration, as well t_1 and t_2 are any two points in time (milliseconds) during the crash while $t = t_2 - t_1$ and $t \le 15(ms)$:

$$SI = \int_0^T a^{2.5} dt = c \tag{22}$$

$$HIC = \max\left[\frac{1}{t_2 - t_1}\int_{t1}^{t2} a\, dt\right]^{2.5}(t_2 - t_1) \tag{23}$$

According to FMVSS 208, the HIC value calculated from the time history of a 50th percentile male dummy's head should not exceed 1000. Euro NCAP proposed criteria for the HIC value evaluation, as shown in Table 1. Although HIC has no sensitivity to the shape of the acceleration curve and its peak time, it is considered an appropriate criterion for crashworthiness in the automotive industry according to experimental tests,

observations and statistical analysis (Mansoor-Baghaei et al., 2019). Mansoor-Baghaei et al. (2019) studied the effect of acceleration pulse shape on head injuries, and the results showed that a curve with retarded peak acceleration generates more considerable brain strain and, therefore, more severe injury. So, they recommend checking both HIC and brain strain while designing protection systems, especially wherever a retarded acceleration peak may present (Mansoor-Baghaei, et al., 2019).

Table 1 Injury criterion in Euro NCAP headform impact tests (Euro NCAP, 2018)

HIC Lower limit	*HIC Higher limit*	*Performance criterion*
–	650	Green
650	1000	Yellow
1000	1350	Orange
1350	1700	Brown
1700	–	Red

1.4 Airbag folding pattern

The importance of folding patterns in airbag deployment behaviour is cleared in previous researches, particularly for the driver, passenger and other internal airbags. For instance, Malczyk and Adomeit (1995) studied the effect of folding patterns on Out-Of-Position (OOP) occupants. The study sought to examine two different folding patterns for the driver-side airbag in OOP configuration. They reported that the P-fold pattern considerably reduced biomechanical loads in the chest and neck for different OOP configurations (Malczyk and Adomeit, 1995). Similarly, four different patterns and their influence in OOP were investigated by Mao and Appel (2001) and the different characteristics of airbag deployment behaviour were examined. Mroz and Pipkorn (2007) studied the use of origami theory in passenger airbags and its influence on airbag deployment behaviour and passenger injury based on the particle method. The research concludes that the particle method is able to predict airbag behaviour with complicated foldings and that the gas flow significantly influences the airbag unfolding procedure (Mroz and Pipkorn, 2007). Cromvik (2007) also developed an origami-based algorithm for passenger airbag folding. A folding technique for roof rail airbag using Dynfold within LS-PrePost is also proposed by Deshpande et al. (2016).

Although the influence of folding pattern on the driver, passenger and other internal airbags have been investigated previously, so far, no research has been conducted to examine this topic in terms of pedestrian protection airbag. In previous research, authors have implemented and validated the corpuscular particle method for pedestrian airbag simulation. The method makes it feasible to simulate inflator gas flow and investigate the gas flow effect on the dynamic behaviour of the airbag and eventually pedestrian head injuries. The current research sought to employ the method implemented previously by authors in order to study the effect of different pedestrian airbag folding patterns on deployment behaviour of the airbag and pedestrian head injuries.

2 Methodology

Previous research on the implementation of the Corpuscular Particle Method (CPM) for Pedestrian Protection Airbag (PPA) simulation was conducted by the authors. A PPA employing centre spurt type inflator was designed to cover the bottom of the windscreen and A-pillars (see Figure 5). An adult headform was impacted to nine points in this area as shown in Figure 4 as P1 to P9. In order to install the PPA on the vehicle FE model a two-stage folding consisting of a flat fold and a spiral fold was proposed as illustrated in Figures 6 and 7. In presence of gravity, impact velocity was equal to 40 km/h and impact angle 65°. Table 2 represents the material properties of the fabric used as airbag cushion. A guanidine nitrate ($CH_6N_4O_3$) based propellant chosen for inflator and nozzle vector was considered to be in the longitudinal direction of the vehicle. Table 3 shows the products and their percentage. The maximum total mass flow rate of the gases was considered to be equal to 6.76×10^{-3} kg/ms, Figure 8 shows the mass flow rate curve of each gas component considered in this paper. Gas temperature, by the way, was considered to be constant and equal to 464° K. Additionally, other properties of the CPM card are declared in Table 4. In order to simulate the PPA, no vent holes were considered in airbag geometry (Deabae and Marzbanrad, 2021).

Figure 4 Impact points for the headform test (Lim et al., 2014)

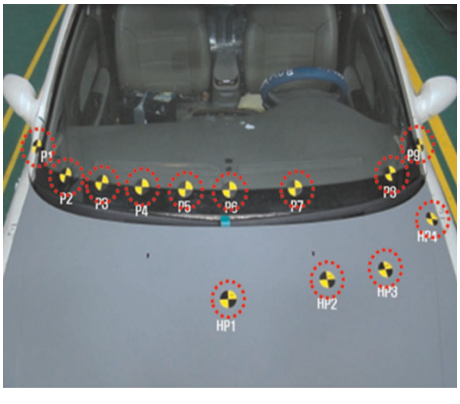

Figure 5 Pedestrian protection airbag (PPA) (Deabae and Marzbanrad, 2021)

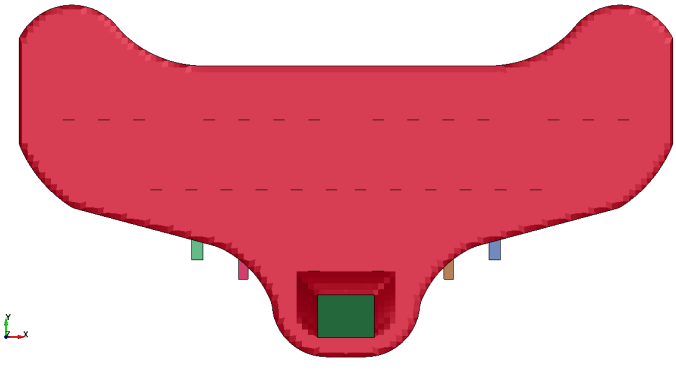

Figure 6 Flat folded pedestrian protection airbag (Deabae and Marzbanrad, 2021)

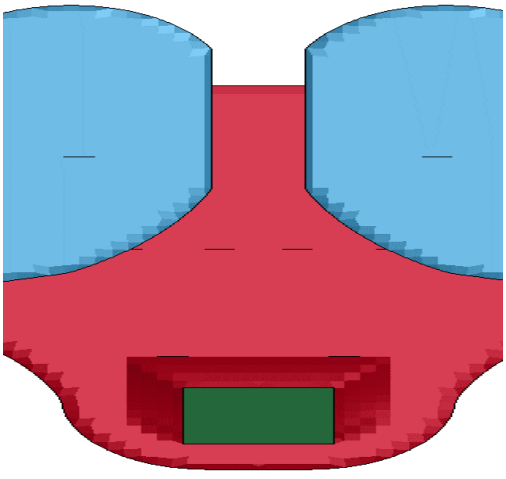

Figure 7 Rolled pedestrian protection airbag (Deabae and Marzbanrad, 2021)

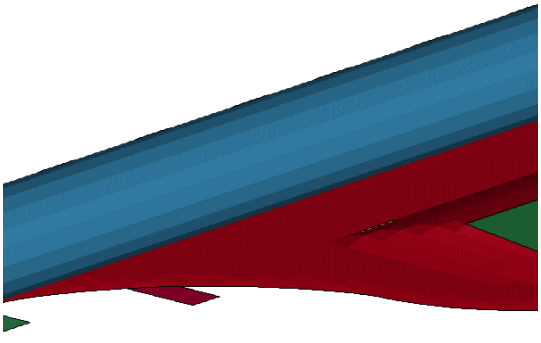

Table 2 Material properties of airbag fabric (Lim et al., 2014)

Density	$8.54\times10^{-7}\left(\frac{\text{kg}}{\text{mm}^3}\right)$
Young's modulus	$0.2(\text{GPa})$
Thickness	$0.33(\text{mm})$
Permeability	1.2
Poisson's ratio	0.2

Table 3 Gaseous products of the guanidine nitrate propellant (Seo et al., 2011)

H_2O	53%
N_2	32%
Co_2	15%

Figure 8 The mass flow rate of different gasses by their percentage of total mass flow rate (Deabae and Marzbanrad, 2021)

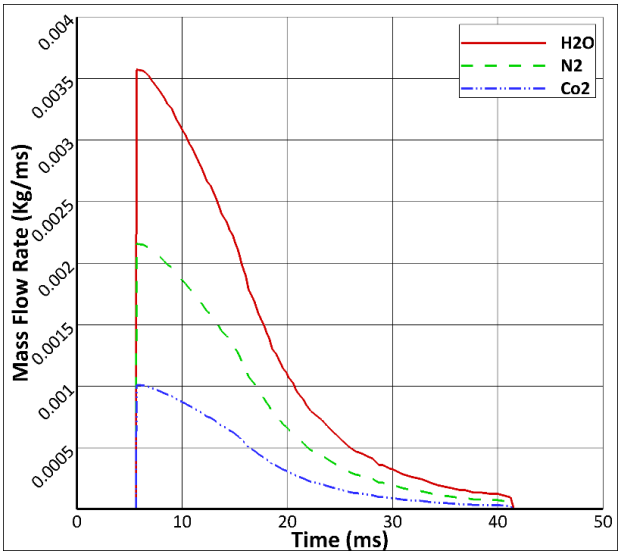

Table 4 CPM card properties (Deabae and Marzbanrad, 2021)

Number of particles	500,000
Atmospheric temperature	293°K
Atmospheric pressure	1.013×10^{-4} GPa

2.1 Airbag folding patterns

Six different folding patterns are considered in the present research to investigate their effect on PPA's unfolding behaviour and pedestrian head injuries. For each pattern an adult pedestrian headform impact into nine points on the bottom of the windshield and on A-pillars, as shown in Figure 4, was simulated. Headform velocity and acceleration time history were exported in each case and HIC values were calculated. Figure 5 shows the pedestrian protection airbag before folding. All selected folding patterns are applied in two consecutive steps. Six folding methods considered in the present study consists of

- Folding-Rolling (FL-RL)
- Rolling-Folding (RL-FL)
- Folding-Z_Folding (FL-ZF)
- Z_Folding-Folding (ZF-FL)
- Folding-Stochastic (FL-ST)
- Rolling-Stochastic (RL-ST)

Folding-Rolling (FL-RL): For this folding pattern the PPA firstly folded in the lateral direction, so that both side sections lay above the middle section as shown in Figure 6. For the second step, the PPA rolled in its lateral direction as shown in Figure 7.

Rolling-Folding (RL-FL): In this method, the steps in the previous one reversed, the PPA rolled in the lateral direction as shown in Figure 9 and then the folding applied to PPA in the lateral direction as shown in Figure 10 using a special folding tool.

Figure 9 Rolled pedestrian protection airbag

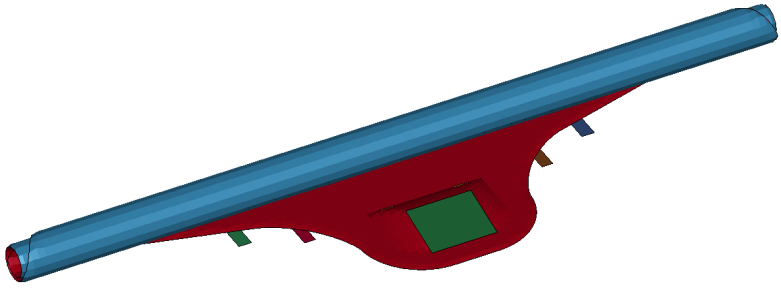

Figure 10 Rolled-Folded pedestrian protection airbag

Folding-Z_Folding (FL-ZF): In this folding pattern a folding is applied to PPA as the first step like the first folding method (see Figure 6) and then the PPA folded in a *Z*-like shape using a specially designed tool for this purpose, the *Z*-fold gives the airbag an accordion-like shape (see Figure 11).

Figure 11 The Folded-Z_Folded pedestrian protection airbag

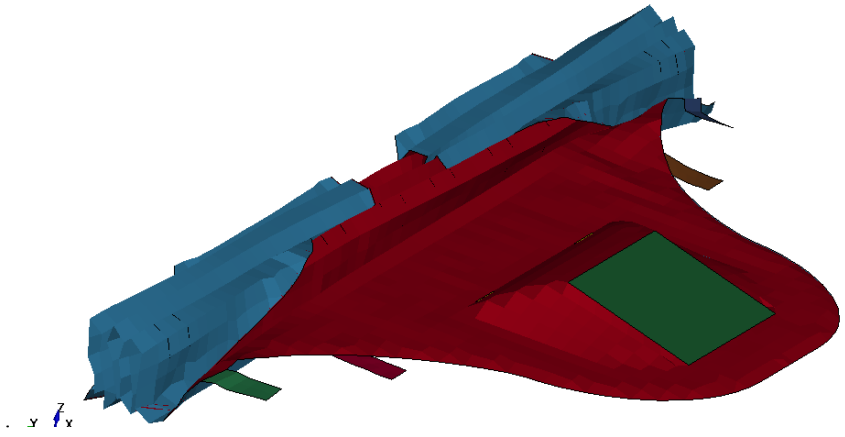

Z_Folding-Folding (ZF-FL): The steps in the previous method applied in reverse in this one. As shown in Figure 12 a special tool designed for Z_Folding folds the PPA in the first stage and the flat fold tool is utilised to fold the airbag in the lateral direction as shown in Figure 13.

Figure 12 Z_Folded pedestrian protection airbag

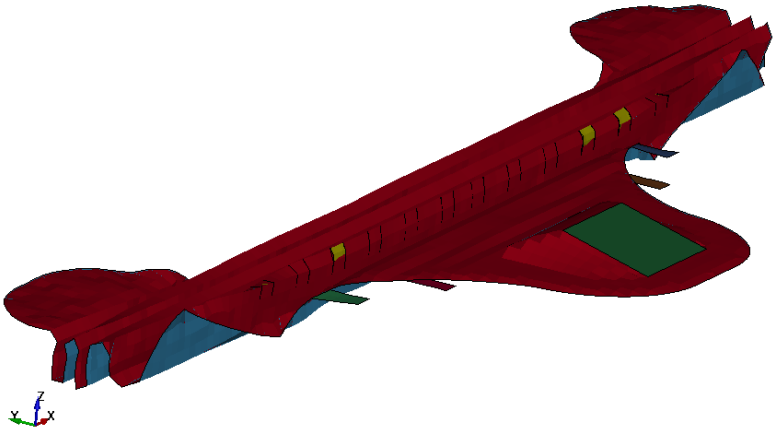

Folding-Stochastic (FL-ST): In this method, a folded airbag as shown in Figure 6 aggregated stochastically to get the pedestrian airbag as shown in Figure 14. In the second step for aggregating the airbag stochastically a box type tool was designed that its size could change over time. Box's width reduced while the folded airbag was placed inside it.

Figure 13 Z_Folded-Folded pedestrian protection airbag

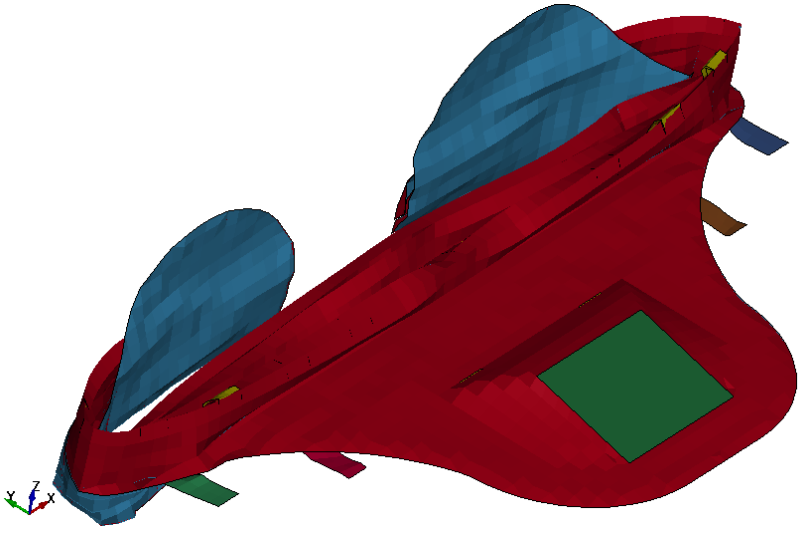

Figure 14 Folded-Stochastic pedestrian protection airbag

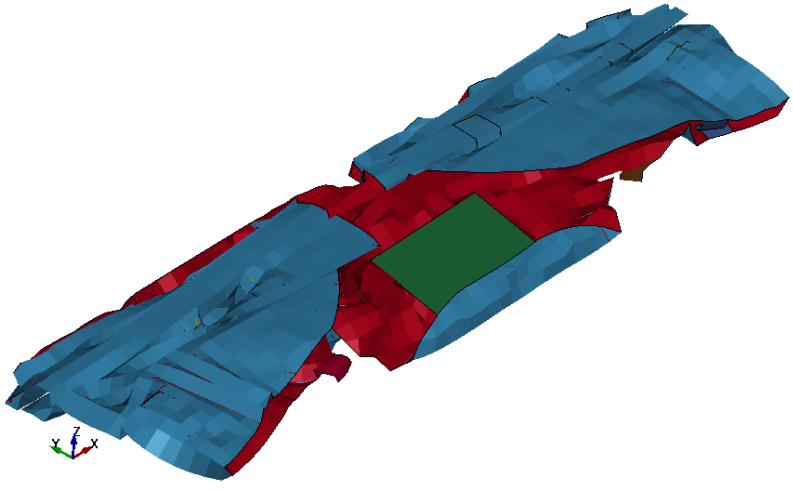

Rolling-Stochastic (RL-ST): Like the previous method in this method a rolled pedestrian protection airbag (see Figure 9) aggregated stochastically and the resulting geometry is shown in Figure 15. The same type of box-like tool is designed in this method too. The rolled airbag is placed inside the box and its length is reduced to meet the final length considered.

Figure 15 Rolling-Stochastic pedestrian protection airbag

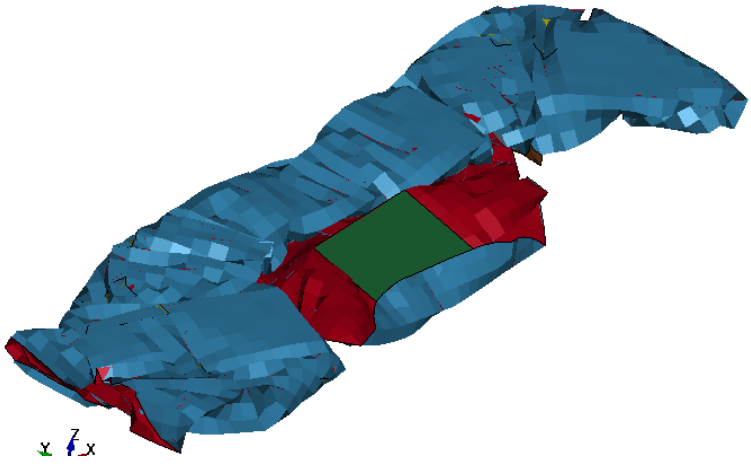

The configuration and simulation details cleared in Section 0 were kept constant to simulate different folding patterns. In other words, only the folding pattern changed for each case.

3 Results and discussion

As mentioned previously, the direct impact of the pedestrian's head into windscreen or A-pillars could generate HIC values up to 7000 that can cause serious injuries, Traumatic Brain Injury (TBI) and death. Equipping vehicles with any pedestrian protection systems could reduce the chance of TBI and death significantly. Pedestrian Protection Airbag (PPA) simulation results reported by authors in previous research show a noteworthy reduction of HIC values while the pedestrian head has been prevented from hitting directly the windshield and A-pillars.

The impact procedure of the headform into the PPA in P6 is shown in Figure 16. Additionally, Figure 17 illustrates the HIC values for the cases with and without PPA. It is reported that a PPA could reduce pedestrian head injuries by up to 90%. The CPM method was also found to be a precise and realistic approach to simulate pedestrian airbag. The method is also proven to be an effective technique to investigate the effect of gas flow on airbag deployment behaviour. Figure 18 shows the time history of the pedestrian headform velocity and acceleration (Deabae and Marzbanrad, 2021).

Figure 16 Headform impact to PPA in point P6 (Deabae and Marzbanrad, 2021)

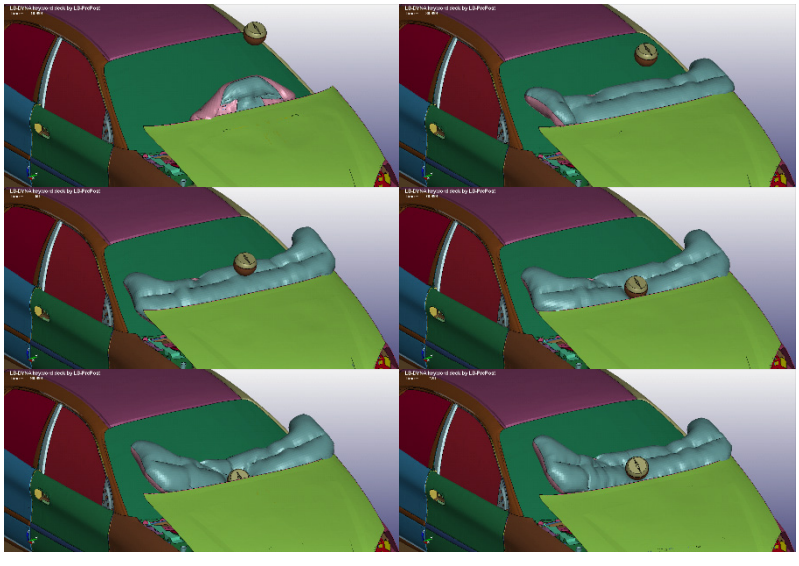

Figure 17 HIC values comparison for headform direct impact to vehicle body and impact to PPA (Deabae and Marzbanrad, 2021)

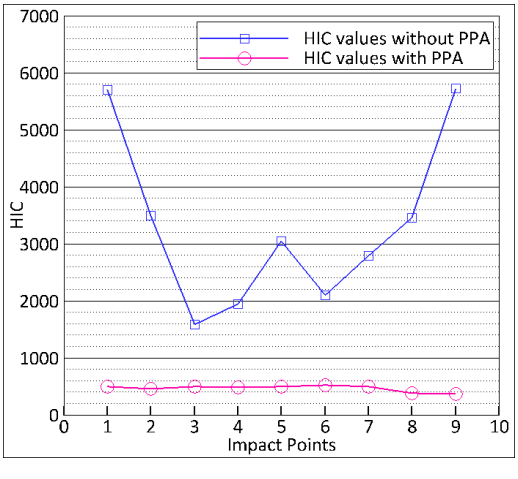

Current research utilised the previously implemented method to investigate the effect of different folding patterns on PPA deployment behaviour and pedestrian head injury.

Figure 18 Headform velocity and acceleration in points P1, P3 and P6 (impact to PPA) (Deabae and Marzbanrad, 2021)

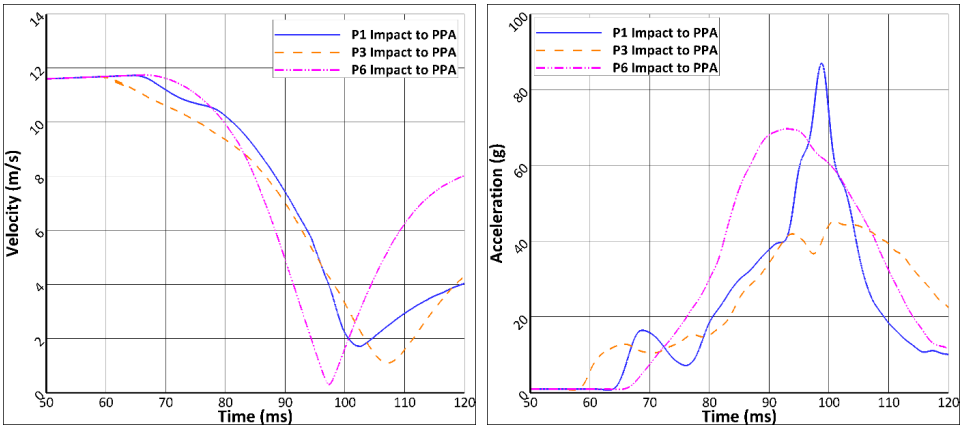

3.1 Effect of folding patterns

Investigating the results of headform impact to six differently folded pedestrian airbags shows that the folding pattern of a pedestrian protection airbag could affect the head injury value by its dynamic behaviour. HIC values for nine points located on the bottom of the windshield and the A-pillars for each folding method were calculated regarding the head acceleration curve. While studying the effect of folding patterns all other influencing parameters were considered to be constant in each case. Figures 19 and 20 show the resulting HIC values from headform impact in nine points for six different folding patterns. In two folding methods, Rolling-Folding and Rolling-Stochastic the headform unfolding is delayed due to the high friction generated between airbag layers and also between airbag and vehicle body, so, they did not deploy completely and headform impacted the A-pillar on point P9. Results show that injuries in the case of using the Folding-Rolling method are less than the other 5 patterns due to the complete deployment of the airbag before headform hit and lower pressure as shown in Figure 21.

Figure 19 Comparison of HIC values for each folding pattern in nine impact points

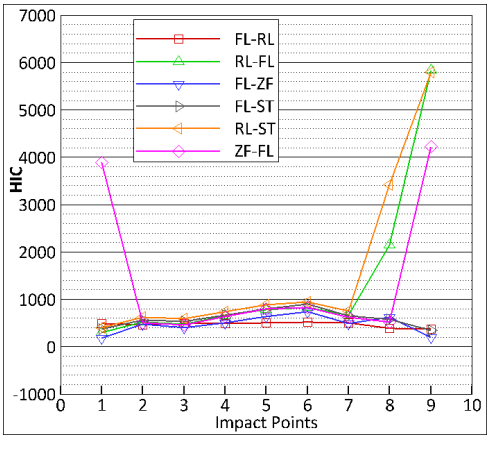

Figure 20 Magnified view of HIC values comparison for each folding method in nine impact points

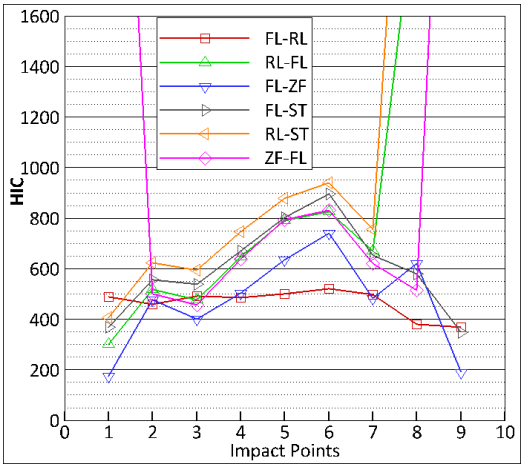

The Rolling-Stochastic method generated higher HIC values than other methods because of higher pressure in the airbag in impact time; also, incomplete deployment of the airbag in this particular case caused the headform to hit the A-pillar on point P9. Additionally, a possible explanation for high airbag pressure, in this case, can also be associated with mentioned incomplete deployment. The Z_Folding-Folding method also caused the headform to deviate and hit the A-pillars in points P1 and P9 because of airbag bounce that happens due to high deployment velocity. This can be explained by the large length of the airbag and the fact that the restraining mechanism considered for the airbag in the current study needs to be placed far from the airbag centreline.

Observing the airbag's internal pressure for six cases in Figure 21 shows that inertia causes the pressure to rise suddenly when inflation starts, then the pressure drops when the airbag starts to unfold. The second rise in airbag pressure is due to the second fold resistance. Airbag's internal pressure is lower in the case of Folding-Rolling that generated the lowest HIC values in comparison with other methods. Similarly, high internal pressure is observed in the Rolling-Stochastic method which its generated HIC values were higher than others. Combining the information from HIC values and the internal pressure of the PPA shows that PPA's internal pressure can affect head injuries directly. The fact that internal pressure of the airbag can significantly affect airbag stiffness and as a result influence head injuries were previously proven by other researchers. So, it is assumed that the mass flow rate of the inflator can affect the internal pressure of the airbag and consequently influence head injuries. On the other hand, the folding pattern of the airbag can considerably affect the internal pressure of the airbag due to the inertia and friction generated between airbag fabric layers, particularly in the early deployment stages.

Figure 21 Internal pressure of PPA for six folding methods

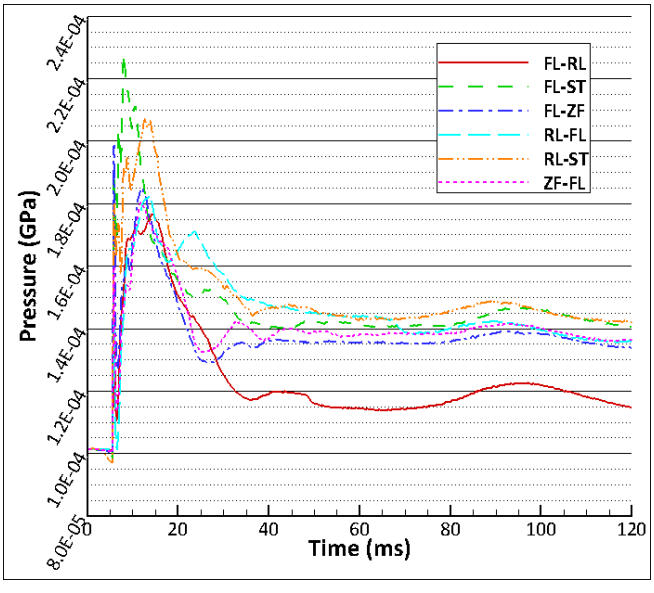

Figure 22 shows the friction energy during the deployment process for each folding pattern; it is clear that the folding pattern of the PPA can affect the frictional energy of the airbag. Moreover, it is obvious that the deployment velocity of the PPA is mostly influenced by frictional energy; as mentioned, the low-friction energy in the case of the Z_Folding-Folding method causes the airbag to deploy very quickly although a bouncing behaviour is observed afterwards. Inspecting frictional energy of the PPA reveals that delayed deployment of the airbag with Rolling-Stochastic and Rolling-Folding methods are also associated with high friction. This comparison shows that while a Z_Folding-Folding pattern is employed inflators with a lower energy rate could be used.

Figure 22 Friction energy comparison for six folding methods of PPA

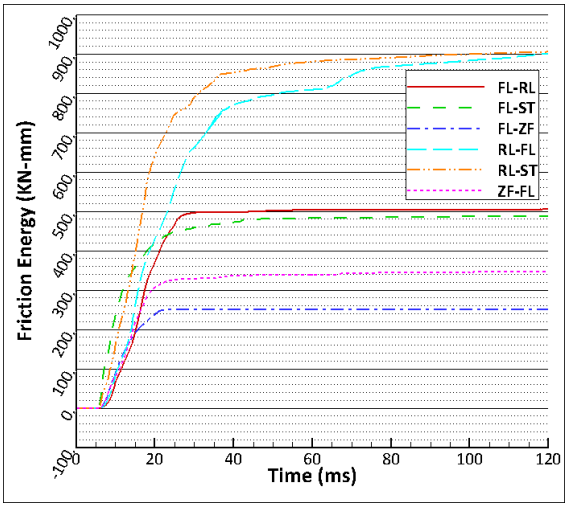

4 Conclusions

In this paper, pedestrian headform's impact into the vehicle's body and to a pedestrian protection airbag was investigated using numerical methods. The simulation results have a good correlation with experimental data reported in the literature. It has been concluded that the impact of the pedestrian's head to the bottom of the windshield and A-pillars could cause severe injuries because of high-acceleration rates. Also, it has been proven that using a pedestrian protection airbag without modifications in the vehicle's front-end structure could lessen the acceleration applied to the head and thus reduce the HIC values by up to 90%.

The Corpuscular Particle Method (CPM) has been utilised in the present work to simulate gas flow entering the pedestrian protection airbag to investigate the effect of flow on the dynamic behaviour of the airbag. CPM seems to be able to predict airbag deployment and unfolding properly, and it could be used for PPA simulation as well as other airbags. Undoubtedly gas flow affects the airbag unfolding procedure and its dynamic behaviour and it could be taken into account whether in the CPM or ALE method. As mentioned, CPM seems to be less time-consuming and more accurate in comparison to ALE. Gas flow direction and the number of particles defined in the CPM also can influence results; it is observed that low particle numbers can lead to noisy results.

Clearly, the folding pattern of the airbag can affect its dynamic behaviour and consequently the injury of the impacting head. Investigating the effect of folding methods on head injuries for a Pedestrian Protection Airbag (PPA) revealed that the Folding-Rolling method generated fewer injuries in the pedestrian's head and absorbed the kinetic energy of the headform better than other folding methods. The Z_Folding-Folding caused the lowest friction energy and deployed faster than the other five patterns, but high unfolding velocity caused a bounce in the airbag deviating the headform towards the A-pillars. The highest friction energy was observed in Rolling-Stochastic and Rolling-Folding, respectively. Additionally, the delayed unfolding of the airbag in both cases due to high friction caused the headform to impact the A-pillars directly.

References

Anantharaju, N., Uduma, K. and Shi, Y. (2020) *Evaluation of Corpuscular Particle Method (CPM) in LS-Dyna for Airbag Modeling*, SAE Technical Paper.

Beles, H. et al. (2019) 'The assessment of pedestrian's head injury risk at the contact with the vehicle's hood', IOP *Conference Series: Materials Science and Engineering*, Oradea, Romania.

Chen, P., Zeng, W. and Yu, G. (2019) 'Assessing right-turning vehicle-pedestrian conflicts at intersections using an integrated microscopic simulation model', *Accident Analysis and Prevention,* Vol. 129, pp.211–224.

Choi, S., Jang, J., Oh, C. and Park, G. (2016) 'Safety benefits of integrated pedestrian protection systems', *International Journal of Automotive Technology*, Vol. 17, No. 3, pp.473–482.

Cromvik, C. (2007) *Numerical Folding of Airbags Based on Optimization and Origami*, Chalmers University of Technology and Goteborg University, Goteborg, Sweden.

Deabae, R. and Marzbanrad, J. (2021) 'Design and simulation of a pedestrian protection airbag using corpuscular particle method', *International Journal of Vehicle Design*, Vol. 86, pp.162–187.

Decker, W. et al. (2019) 'Evaluation of finite element human body models for use in a standardized protocol for pedestrian safety assessment', *Traffic Injury Prevention*, Vol. 20, pp.S32–S36.

Deshpande, V.C., Lian, W. and Nair, A. (2016) *Roof Rail Airbag Folding Technique in LS-PrePost Using DynFold Option*, Detroit, USA, s.n.

Euro NCAP (2018) *Pedestrian Testing Protocol*, s.l.: European New Car Assessment Programme (Euro NCAP).

Han, Y. et al. (2017) '*Analysis* of vulnerable road user kinematics before/during/after vehicle collisions based on video records', *IRCOBI Conference Proceedings*, Antwerp, Belgium.

Hirth, A., Haufe, A. and Olovsson, L. (2007) *Airbag Simulation with LS-DYNA Past – Present – Future*, Gothenburg, s.n.

Huang, S. and Yang, J. (2010) 'Optimization of a reversible hood for protecting a pedestrian's head during car collisions', *Accident Analysis and Prevention,* Vol. 42, pp.1136–1143.

Jakobsson, L., Fredriksson, A. and Lindman, M. (2013) *Pedestrian Airbag Technology – A Production System*, Seoul, Republic of Korea, s.n.

Krenn, M. et al. (2003) *Development and Evaluation of a Kinematic Hood for Pedestrian Protection*, Detroit, Michigan, s.n.

Lalwala, M., Chawla, A., Thomas, P. and Mukherjee, S. (2019) 'Finite element reconstruction of real-world pedestrian accidents using THUMS pedestrian model', *International Journal of Crashworthiness*, Vol. 25, No. 4, pp.360–375.

Lee, T-H., Yoon, G-H., Han, M-S. and Choi, S-B. (2018) 'Shock mitigation of pedestrians from sports utility vehicles impact using active pop-up and extended hood mechanisms: experimental work', *Proceedings of the Institution of Mechanical Engineers, Part D: Journal of Automobile Engineering*, Vol. 232, No. 12, pp.1573–1583.

Lian, W., Bhalsod, D. and Olovsson, L. (2008) *Benchmark Study on the AIRBAG_PARTICLE Method for Out-Of-Position Applications*, Detroit, s.n.

Li, G., Yang, J. and Simms, C. (2017) 'Safer passenger car front shapes for pedestrians: a computational approach to reduce overall pedestrian injury risk in realistic impact scenarios', *Accident Analysis and Prevention*, Vol. 100, pp.97–110.

Lim, J-H. et al. (2014) 'Design of an airbag system of a mid-sized automobile for pedestrian protection', *Journal of Automobile Engineering*, Vol. 229, No. 5, pp.656–669.

Lin, C-H. and Cheng, Y-P. (2018) *Evaluation of LS-DYNA® Corpuscular Particle Method – Passenger Airbag Applications*, Detroit, s.n.

Lin, C-H., Cheng, Y-P. and Wang, J. (2014) *Evaluation of LS-DYNA® Corpuscular Particle Method for Side Impact Airbag Deployment Applications*, Detroit, s.n.

Liu, W. et al. (2019) 'Parameter sensitivity analysis of pedestrian head dynamic response and injuries based on coupling simulations', *Science Progress*, Vol. 103, No. 1. Doi: 10.1177/0036850419892462.

Longhitano, D. et al. (2005) *Influence of Vehicle Body Type on Pedestrian Injury Distribution*, Detroit, Michigan, s.n.

Lu, Y. et al. (2020) 'Studying on the design and simulation of collision protection system between vehicle and pedestrian', *International Journal of Distributed Sensor Networks*, Vol. 16, No. 1. Doi: 10.1177/1550147719900109.

Malczyk, A. and Adomeit, H-D. (1995) *The Airbag Folding Pattern as a Means for Injury Reduction of Out-of-Position Occupants*, Warrendale, USA, s.n.

Mansoor-Baghaei, S., Sadegh, A.M. and Charles, S. (2019) 'Characteristics of HIC in prediction of mTBI relating to crash pulses', *Int. J. Vehicle Design*, Vol. 80, No. 1, pp.59–85.

Mao, Y. and Appel, H. (2001) *Influence of Air Bag Folding Pattern on OOP-injury Potential*, Warrendale, USA, s.n.

Meng, Y. et al. (2016) 'A 6 year-old pediatric finite element model for simulating pedestrian impacts', *Proceedings of the14th International LS-DYNA Users Conference*, Detroit, pp.1–10.

Meng, Y. et al. (2017) 'A finite element model of a six-year-old child for simulating pedestrian accidents', *Accident Analysis and Prevention*, Vol. 98, pp.206–213.

Mroz, K. and Pipkorn, B. (2007) *Mathematical Modelling of the Early Phase Deployment of a Passenger Airbag – Folding Using Origami Theory and Inflation Using LS-DYNA Particle Method*, Gothenburg, s.n.

Nagatomi, K. et al. (2005) *Development and Full-Scale Dummy Tests of a Pop-Up Hood System for Pedestrian Protection*, Washington D.C, s.n.

Olovsson, L. (2007) 'Corpuscular method for airbag deployment simulations', *Proceedings of the 6th European LS-DYNA Conference*, Gothenburg.

Pak, W. et al. (2018) 'Preliminary validation of a detailed finite element model of a 50th percentile male pedestrian', *Proceedings of the 15th International LS-DYNA Conference*, Detroit.

Pak, W. et al. (2019) 'Finite element model of a high-stature male pedestrian for simulating car-to-pedestrian collisions', *International Journal of Automotive Technology*, Vol. 20, No. 3, pp.445–453.

Seo, Y-D., Chung, S.H. and Yoh, J.J. (2011) 'Automotive airbag inflator analysis using the measured properties of modern propellants', *Fuel*, Vol. 90, pp.1395–1401.

Severy, D.M. (1970) *State-of-the-Art Vehicle Exterior Safety*, s.l., s.n.

Shin, M-K., Park, K-T. and Park, G-J. (2008) 'Design of the active hood lift system using orthogonal arrays', *Journal of Automobile Engineering*, Vol. 222, pp.705–717.

Sun, M., Sun, X. and Shan, D. (2019) 'Pedestrian crash analysis with latent class clustering method', *Accident Analysis and Prevention*, Vol. 124, pp.50–57.

Takahashi, H. et al. (2013) *Development of Pop-Up Hood System for Pedestrian Protection*, Seoul, Republic of Korea, s.n.

Untaroiu, C.D. et al. (2018a) *A Study of Pedestrian Kinematics and Injury Outcomes Caused by a Traffic Accident with Respect to Pedestrian Anthropometry, Vehicle Shape, and Pre-Impact Conditions*, Detroit, s.n.

Untaroiu, C.D. et al. (2018b) 'A finite element model of a mid-size male for simulating pedestrian accidents', *Journal of Biomechanical Engineering*, Vol. 140, No. 1. Doi: 10.1115/1.4037854.

Vyas, G.M., Andre, A. and Sala, R. (2019) 'Toward lightweight smart automotive hood structures for head impact mitigation: integration of active stiffness control composites', *Journal of Intelligent Material Systems and Structures*, Vol. 31, No. 1, pp.71–83.

Wang, J. and Teng, H. (2010) *The Recent Progress and Potential Applications of CPM Particle Method in LS-DYNA*, Bamberg, s.n.

Wang, J.T. and Nefske, D.J. (1988) *A New CAL3D Airbag Inflation Model*, Detroit, s.n.

Wetzstein, I., Lauterbach, B., Erzgräber, M. and Harzheim, L. (2015) *Optimization of a Lower Bumper Support Regarding Pedestrian Protection Requirements using ANSA and LS-Opt*, Würzburg, Germany, s.n.

World Health Organization (2018) *Global Status Report on Road Safety 2018*, World Health Organization, s.l.

Yang, F. and Beadle, M. (2015) *CAE Analysis of Passenger Airbag Bursting through Instrumental Panel Based on Corpuscular Particle Method*, Würzburg, s.n.

Yang, H-I., Yun, Y-W. and Park, G-J. (2015) 'Design of a pedestrian protection airbag system using experiments', *Proceedings of the Institution of Mechanical Engineers, Part D: Journal of Automobile Engineering*, Vol. 230, No. 9, pp.1182–1195.

Yüksel, A., Aras, F. and Çolpan, O. (2017) *Head Impact Analysis Validation for Aluminium Bonnet*, Salzburg, Austria, s.n.

Zeng, X., Peng, X., Lu, H. and Pasquale, E.D. (2014) *Optimization Design of Bonnet Inner Based on Pedestrian Head Protection and Stiffness Requirements*, Detroit, s.n.

Zou, T., Zha, A., Liu, Q. and Simms, C. (2020) 'Pedestrian gaits observed from actual pedestrian-vehicle collisions', *International Journal of Crashworthiness*, pp.1–23.